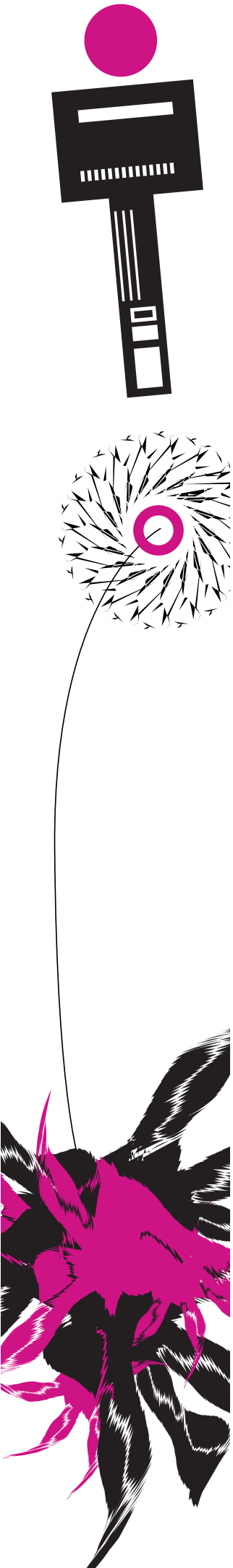

RAM ROBOTICS AND MECHATRONICS

THE DYNAMICS OF TAIL-SUPPORTED CLIMBING IN ROBOTICS AND BIRDS

N. (Nart) Pistorius

MSC ASSIGNMENT

Committee:
prof. dr. ir. G.J.M. Krijnen
ir. A.P. Dijkshoorn
ir. R.S.M. Sneep
dr. ir. R.G.K.M. Aarts

October, 2022

046RaM2022
Robotics and Mechatronics
EEMathCS
University of Twente
P.O. Box 217
7500 AE Enschede
The Netherlands

UNIVERSITY OF TWENTE. | TECHMED CENTRE UNIVERSITY OF TWENTE. | DIGITAL SOCIETY INSTITUTE

Acknowledgement

The research presented is an important personal milestone and is the end of a wonderful journey to obtain the master's degree in Electrical Engineering at the Univeristy of Twente. During this journey, I got acquainted with many interesting friends in the field. I am looking forward to apply the gained knowledge in industry. The achievements I could have never done without the people who supported me.

Firstly, I would like to thank ir. A. Dijkshoorn, ir. R. Sneep and prof.dr.ir. G. Krijnen for their continued feedback and excellent guidance during the thesis process. Their experience has helped to guide the research more effectively and their critical thinking always provided useful feedback.

Secondly, I would like to thank my family and friends who have encouraged and supported me all the way, regardless of what happened.

Contents

1 Paper

The following pages show the core of the research, presented as a separate paper.

A study into the kinematic and the dynamics of tail-supported climbing in robotics and birds

Nart Pistorius, n.pistorius@student.utwente.nl
University of Twente 2022, Electrical Engineering, Dept. RaM

***Abstract*— This work explores the dynamics of actively using a tail for climbing a vertical surface. In nature, woodpeckers, woodcreepers and treecreepers climb vertical tree trunks suspended by their feet and supported by their tail. Videos of these climbing birds are analysed. In general, the stride is initiated by the body pitching forward while simultaneously moving towards the trunk and accelerating up before lifting off. A 2D planar rigid body model is presented and the trajectory for the minimal cost of transport is determined by solving a constrained nonlinear problem. The limiting factors and driving parameters of this legged locomotion gait are investigated. The locomotion efficiency reduces when the jump height and jump time approach the ballistic limit. This work gives a first step towards understanding the role of tail support in climbing dynamics.**

Keywords: Tail-supported climbing, bio-inspired, Cost of Transport, optimisation, legged locomotion, climbing robots

I. Introduction

Energy efficiency is a primary concern for mobile robots. For example, small aerial robots are limited by short mission time because of high energy usage [1], [2]. To extend the mission time a robot could perch on a surface as biological flyers do [3]. Beyond perching, biological flyers are capable of manoeuvring on the surface to explore, inspect and forage. The multiple modes of operation, with flying mode, touch down followed by surface locomotion mode, to take off and go fly again, are an inspiration for robot design toward better energy utilisation depending on the given task [2]. This work focuses on vertical surface locomotion. The style of movement of this mode is inspired by climbing birds in trees which use their tail actively in a jumping locomotion strategy [4] [5].

Many small-bodied birds of the order Passeriformes, also known as perching birds, are capable of climbing and/or clinging to some extent. However, there is a group that is considered specialists in tree trunk climbing, existing of woodpeckers (of order Piciformes and family Picidae), woodcreepers (of order Passeriformes and family Furnariidae), nuthatches (of order Passeriformes and family Sattidae) and treecreepers (of order Passeriformes and family Certhidae) [4].

Within this group, there are different climbing gaits and skills. The woodpeckers, woodcreepers and treecreepers are only reported to climb upwards by means of jumping, with the aid of tail [6] [5]. Whereas nuthatches are reported to be able to locomote by walking [7] and jumping/hopping [8] up- and downwards without tail support on vertical substrates [9]. The woodpeckers, woodcreepers and treecreepers have morphological adaptations for climbing, for example, they are equipped with stiffened tail feathers, long curved claws and strong leg-flexor muscles [6] [5] [10] [11].

The locomotion gait of a treecreeper is studied in depth by Norberg [6] and exists of 2 distinct phases, the power stroke (propulsive stroke), and the floating phase (recovery stroke). In the first phase, the bird is slipping closer to the trunk by rotating around the hip joint and at the same time possibly pulling the hip slightly towards the trunk by the legs. In the second phase, the bird is in free flight before reattaching and hanging still again.

The tree trunk climbing birds outperform current state-of-the-art climbing robots in many ways, like climbing velocity and manoeuvrability. However, as the field of robotics research has made advancements, climbing robots have become faster, lighter, smaller and more efficient. Two essential aspects in this field are attachment strategy (magnetic, pneumatic, mechanical, chemical and hybrid) and locomotion strategy (wheeled, tracked, walking and hybrid) [12].

Various locomotion strategies for climbing robots have been studied and developed with a tail. The tail is mostly used to compensate for pitch-back moments produced by having a center of mass some distance out from the wall [13].

Locomotion strategies based on multiple side-way arms are studied, e.g. the four-legged robot of [14] inspired by a gecko, or the six-legged RiSE robot [15] inspired by a gecko and cockroach. The climbing gait of these robots is limited by the number of feet that can be detached while climbing, Which is a disadvantage for the flexibility and manoeuvrability of the robot. Furthermore, there are robots that use 2 arms in front to drag themselves up, pulling up with 1 arm before reaching out with the other arm higher up [16] [13]. Also, there are robots vertically climbing with horizontal movement of CoM (swinging). They are hanging on 2 points. The robot of [17] has 2 2-DOF arms, by sequentially changing the pivot point of the pendulum, the swing changes. The ROCR robot [18] has fixed arms, the robot climbs by actively swinging the CoM/tail.

A shortcoming of these robots is that they can not manoeuvre large gaps, high hurdles, a forest or a single tree, which does not seem to be a problem for the tree trunk climbing birds. By having a jumping locomotion strategy, it allows the birds to move quickly and easily over rough surfaces. Hence, the jumping locomotion is more agile compared to other locomotion strategies.

Agile jumping locomotion on ground level with a standstill between each stride is inefficient because all potential energy

is dissipated by each standstill. Therefore a continuous hopping motion with energy storage in a spring is more energy efficient. But in vertical climbing the halt between each stride is no disadvantage since the kinetic energy has all been converted into potential energy by the end of the floating phase, i.e. it has all been used for progression upwards along the trunk. [6].

The energy efficiency of locomotion is frequently quantified by the cost of transport (CoT), this is the amount of energy used per distance travelled, sometimes also referred to as specific resistance [19]. The CoT is a dimensionless quantity, therefore allowing comparison between animal and robotic transportation, and different transportation modes, jumping, flying and walking. In previous research, the CoT is used for selecting gaits for economical locomotion of legged robots [20]. Humans for example tend to choose speeds [21] and step length [22] to minimise CoT.

This work investigates the kinematics and dynamics of tail-supported climbing. Therefore the governing dynamics of tail-supported climbing are analysed to investigate potential adoption for robotic climbers. The relation between energy efficiency, stride length and stride time is explored. The influence of parameters like damping and holding torque are covered. To investigate the benefits of tail-supported climbing, a comparison is made for climbing without tail-support.

To explore the benefits of tail-supported climbing, videos of climbing birds are analysed and used to obtain the governing kinematics. The method used for this is explained in section II-A. Next, to investigate if we can learn from the kinematics, a model is established and the method of modelling is covered in section II-B. Followed by section II-C, explaining the method used to determine the optimal trajectory for a minimal cost of transport. The results of the kinematics of video are presented in section III-A, followed by results of optimal trajectory for the model given in section II-C. The results are compared and discussed in section IV. This work is concluded with conclusion in section V.

II. Methods

A. Video analysis

To study the kinematics, we analyse videos of tree trunk climbers, treecreepers and woodpeckers. We consider these movements as the ground truth. Birds are evolved for multiple things. But they are successful at jumping climbing, since they use it to forage.

First various videos are collected, next to extract the information the steps are executed.

1) Video collection & Materials: Videos of climbing woodpeckers and treecreepers (tab I) are obtained via YouTube, The Macaulay Library at the Cornell Lab of Ornithology, written literature and self-recorded. The selected videos meet two main requirements. First, the bird is climbing on a vertical substrate. The second is that the perspective is 'en profil'. The collection exists of 8 individual birds and 13 jumps, some birds jump multiple times in one video. The videos obtained via YouTube and MacaulayLibrary predominately have a frame rate of 30 Hz. Since the majority of the birds complete a cycle within 0.5 s, only at most 15 frames are captured of the cycle in these videos. The frame rate of the self-recorded video with a high-speed (Phantom VEO 710L, 12x zoom lens) camera is 400 Hz [23].

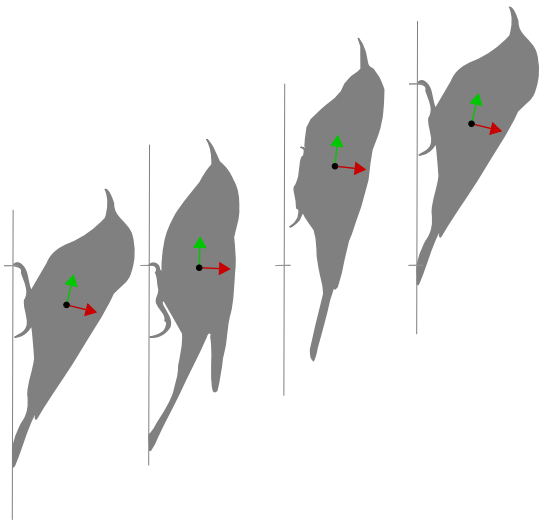

Fig. 1: Climbing gait against time, (a) with the position at start time, (b) position rotated and translated at acceleration phase, (c) position at free-flying phase and (d) position at end of stride (treecreeper [6])

2) Position tracking: Video frames are stabilised such that the background is static in the image frame, does not zoom in or out, rotate and translate (similarity transformation). Implemented with MATLAB's video processing toolbox, feature points are detected in the first frame in a selected region in the image frame (background) with minimum eigenvalue algorithm [33]. The detected points are tracked in the subsequent frames. Based on matching points between the first and following frames geometric transformation is estimated and applied to the frame such that is stabilised.

For every frame, an ellipse (with the same dimensions for every frame) is fitted (by eye) on top of the bird's body. The positions and orientations (x, y, φ) of the ellipse are saved.

The positions and orientations of the bird in image frame coordinates are scaled to SI units using the length from the bill-tip to the tail-tip for the particular species. The lengths of species are given by a range tab. I. The jump height and jump time can be estimated to determine the jump velocity.

To investigate if the birds climb with a common gait we normalise the positions (x, y) with the jump height Δy. The normalisation is implemented because the characteristics of the jumps, like jump height, position in time and initial- and end position, are varying between jumps of the same individual, other individuals of the same species and between species. The variations could be based on what the bird is doing, the dimensions of the bird and the local environment. By normalising the positions and taking the average over the positions we can determine the trend in the climbing gait.

TABLE I: Birds used for video analysis

Number	Species	Number of jumps	Frame rate	Bill-tip length	Mass
1	Hairy woodpecker [24]	1	30 Hz	18-26cm	40-95g [25]
2-5	Pileated woodpecker [26]	4	30 Hz	40-49cm	250-350g [27]
6	Pileated woodpecker [28]	2	30 Hz	40-49cm	250-350g
7-9	Pileated woodpecker [29]	3	30 Hz	40-49cm	250-350g
10	Brown creeper [30]	1	50 Hz	12-14cm	5-10g [31]
11	Spotted woodpecker [32]	1	30 Hz	22–23cm	70–90g [**?**]
12	Treecreeper Norberg [6]	1	80 Hz	12cm	9g [6]
13	Spotted Woodpecker [23]	1	400 Hz	22–23cm	70–90g [32]

To be able to take the average, the positions are linearly interpolated such the number of samples is the same.

3) Inverse dynamics: We can find the velocity by numerically differentiating the position, and by differentiating once again to obtain the acceleration. By estimating the mass matrix (by taking an ellipsoid with certain dimensions), and applying inverse dynamics, the net forces can be determined [34]. If the bird is only in contact with the surface at one point, for example when only the feet are in contact with the surface and treating both feet as 1 contact (since they are a symmetrical and synchronous contact), then all net forces are counteracted by the surface contact force at the contact point. If the bird is in contact with the feet and the tail, considering this as 2 contacts, then we would not accurately obtain the contact forces. By not knowing the contact forces, we would do not know the forces acting on the body. We could only know the net forces.

4) Sources of noise: Some sources of noise are identified here to be aware of the uncertainties in the measurement results. The errors and uncertainties in the measurement of the position and orientation in the video are introduced by the ellipse not being accurate as mass estimation, human eye error of placing the ellipse at the right location, the tree not being vertical, the bird not jumping strictly vertically but also sideways around the tree, the error due to camera calibration and the camera perspective. Yet these noise sources are relatively small compared to the scaling range with the length reported I.

5) Ballistic limit: The results of the measurements (jump height and jump time) are expected to be below the ballistic limit [35]. This limit is given by an object with initial upward velocity v_0 decelerated by gravity g. The velocity as a function of time of this object is

$$\dot{y}(t) = \dot{y}_0 - gt, \tag{1}$$

resulting in the height y as function of time

$$y(t) = \dot{y}_0 t - \frac{1}{2} g t^2 + y_0. \tag{2}$$

The height is maximum for $\dot{y} = 0$, yielding $v_0 = gt$, hence the jump height should be limited by $\Delta y \leq (1/2) g \Delta t^2$.

If the bird would go from standstill to vertical velocity $\dot{y}_0$ instantaneously, the maximum jump height is given Δy. But creating instantaneous velocity is not likely, since the mass is not zero. Thus the jump height should be below the ballistic limit.

Other forms of vertical locomotion, climbing, running uphill, flapping flight, drones are not subject to the ballistic limit, because flapping flight and drones are able to propel while flying. And continuous climbing and running uphill does not come to standstill before the next cycle and does not have a flying phase.

B. Model

To study the dynamics of tail-supported climbing in robotics a model is established. An overview of the modelling choices is given next, followed by a method used to model the rigid body dynamics, the contact forces and the non-elastic impact.

1) Overview of modelling: The robot is modelled as a 2D planar rigid body robot in contact with a rigid wall. There is no elasticity modelled at all, not at the joints and not at interaction with the vertical surface. The legs are modelled as 1 leg since the legs are moving synchronously. The head is not considered in this model. The legs of the robot are able to span a 2D plane, to restrict the radius of the plane it is chosen to model the legs by 2 leg segments with 2 rotational joints, as shown in fig. 2. There is not a rotational actuated joint located in the foot (as an ankle joint). The foot can rotate but is not actuated. This has 2 reasons, first, the ankle joint in nature, specifically for the treecreeper, does not seem to be able to produce significant power, since the legs are thin. The second reason is that the robot does not need an ankle joint to be able to climb. The tail is modelled as a body attached to a rotational joint. Another reason to use all rotational joints is that it is practical to use in a robotic hardware implementation. The contact between foot and surface is modelled as one-point contact.

2) Equations of motion: The main body is described as a floating base, where x, y and φ are the position and orientation of the main body, α_A is the hip joint angle, α_B is the knee joint angle and α_C is the tail joint angle. The states $\mathbf{q}, \dot{\mathbf{q}} \quad \mathrm{R}^n$ can be written in generalised coordinates as

$$\begin{aligned} \mathbf{q} &= \begin{bmatrix} x & y & \varphi & \alpha_A & \alpha_B & \alpha_C \end{bmatrix} \\ \dot{\mathbf{q}} &= \begin{bmatrix} \dot{x} & \dot{y} & \dot{\varphi} & \dot{\alpha_A} & \dot{\alpha_B} & \dot{\alpha_C} \end{bmatrix} . \end{aligned} \tag{3}$$

The hip, knee and tail actuators produce torques τ_A, τ_B and τ_C which are directly coupled to the rigid body. There is not a spring modelled in between the motor and the rigid body (to make a series elastic actuation SEA) for the main reason for simplicity. Furthermore, this would increase the amount of states, and also just create a force, and it could

introduce unwanted oscillatory behaviour. The control forces $\mathbf{u} \in R^n$ in generalised coordinates are

$$\mathbf{u} = \begin{bmatrix} 0 & 0 & 0 & \tau_A & \tau_B & \tau_C \end{bmatrix} - \mathbf{d}\dot{\mathbf{q}} \tag{4}$$

where $\mathbf{d}$ is damping in the joints making the system is not energy conservative, yielding that a positive net work must be performed by the actuators over the course of a stride. Air resistance is neglected. At all joints the damping r is chosen to be identical

$$\mathbf{d} = \begin{bmatrix} 0 & 0 & 0 & r & r & r \end{bmatrix} \tag{5}$$

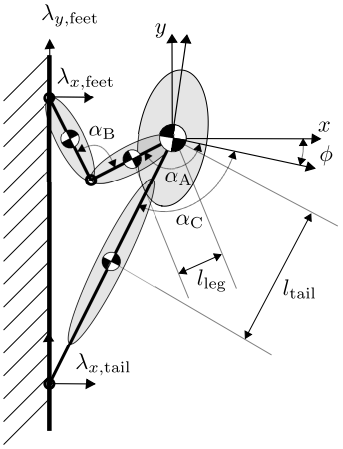

Fig. 2: 2D rigid planar model

The equations of motion of the system (derived from Euler-Lagrange, see appendix) with contact eq. (6) and without contact eq. (7) are

$$\mathbf{M}(\mathbf{q})\ddot{\mathbf{q}} = \mathbf{f}_{cg}(\dot{\mathbf{q}}, \mathbf{q}) + \mathbf{u} + \mathbf{J}^{\top}(\mathbf{q})\lambda \tag{6}$$

$$\mathbf{M}(\mathbf{q})\ddot{\mathbf{q}} = \mathbf{f}_{cg}(\dot{\mathbf{q}}, \mathbf{q}) + \mathbf{u} \tag{7}$$

where $\mathbf{f}_{cg}$ is the Coriolis and gravitational forces, $\mathbf{u}$ is the input forces eq. (4), $\mathbf{J}(\mathbf{q})$ is the contact Jacobian eq. (8) and λ is the contact forces eq. (10).

a) Contact forces: The foot contact is constrained in x and y with no slipping and sliding, the tail contact is only constrained in x, allowing the tail to slide over the surface in y-direction. Hence when the tail or foot are in contact with the surface, the contact velocity $\dot{\mathbf{r}}$ and acceleration $\ddot{\mathbf{r}}$ should be zero

$$\dot{\mathbf{r}} = \begin{bmatrix} \dot{x}_{\text{foot}} \\ \dot{y}_{\text{foot}} \\ \dot{x}_{\text{tail}} \end{bmatrix} = \frac{\partial \mathbf{r}}{\partial \mathbf{q}} \frac{\partial \mathbf{q}}{\partial t} = \mathbf{J}\dot{\mathbf{q}} = 0 \tag{8}$$

$$\ddot{\mathbf{r}} = \mathbf{J}\ddot{\mathbf{q}} + \dot{\mathbf{J}}\dot{\mathbf{q}} = 0 \tag{9}$$

By substituting eq. (6) into eq. (9), the contact forces can be expressed as (dependence of $\mathbf{q}$ is left out for readability)

$$\lambda = \left(\mathbf{J}\mathbf{M}^{-1}\mathbf{J}^{\top}\right)^{-1}\left(-\mathbf{J}\mathbf{M}^{-1}\left(\mathbf{f}_{cg} + \mathbf{u}\right) - \dot{\mathbf{J}}\dot{\mathbf{q}}\right). \tag{10}$$

3) Impact: When contact is made, velocities change instantaneously as a consequence of the zero velocity at the point of contact $\dot{\mathbf{r}}$ right after collision at t^+

$$\mathbf{J}(\mathbf{q}^+)\,\dot{\mathbf{q}}^+ = 0. \tag{11}$$

Assuming that position is approximately the same just before and just after impact $\mathbf{q}^- \approx \mathbf{q}^+$ (because $t^- \approx t^+$), the contact forces can be computed by integrating eq. (6), yielding

$$\mathbf{M}(\mathbf{q})\dot{\mathbf{q}}^+ - \mathbf{M}(\mathbf{q})\dot{\mathbf{q}}^- = \mathbf{J}^{\top}(\mathbf{q}) \int_{t^-}^{t^+} \lambda(t)\mathrm{d}t \tag{12}$$

Left multiplying eq. (12) by $\mathbf{M}^{-1}(\mathbf{q})$, subsequently left multiplication by $\mathbf{J}(\mathbf{q})$ and substitution with eq. (11) results in

$$-\left(\mathbf{J}\mathbf{M}^{-1}\mathbf{J}^{\top}\right)^{-1}\mathbf{J}(\mathbf{q})\dot{\mathbf{q}}^- = \int_{t^-}^{t^+} \lambda(t)\mathrm{d}t \tag{13}$$

Substituting eq. (13) back into eq. (12) allows the expression to be written without the integral, leaving the velocity after impact expressed explicitly by the velocity before impact

$$\dot{\mathbf{q}}^+ = \left(\mathbf{I} - \mathbf{M}^{-1}\mathbf{J}^{\top}\left(\mathbf{J}\mathbf{M}^{-1}\mathbf{J}^{\top}\right)\mathbf{J}\right)\dot{\mathbf{q}}^- \tag{14}$$

In order to handle the discontinuity and the change of equations of motion eq. (6), the integration interval must be divided into predefined stages. In section II-C is explained which method is used to do this.

4) Parameters: In nature, the tree trunk climbing birds vary in mass. The treecreeper with 9 g [6] to the larger woodpeckers with 350 g [27] are all able to climb. The total mass is chosen as 9 g, to be similar to the treecreeper. Assuming that the main body is a homogeneous ellipsoid that is 0.77 % of total mass, and semi axis a and b estimated by Norberg [6], the moment of inertia is $j_b = 1/5 m_b(a^2 + b^2)$. The moment of inertia of a leg segment is chosen as a rod rotating around center $j_{\text{leg}} = 1/12 m_{\text{leg}} l_{\text{leg}}^2$ and for the tail $j_{\text{tail}} = 1/12 m_{\text{tail}} l_{\text{tail}}^2$. Length of legs and tail are chosen to be comparable with data of a treecreeper. The damping is chosen to make the system unconservative.

The contact forces of the foot are unconstrained. The contact force of the tail is constrained to be positive.

C. Optimisation

The optimisation aims to find the control inputs to travel from the start point to the endpoint with the minimal objective function. This trajectory optimisation is transcribed with the dynamics and control input into a non-linear program (NLP) and solved with a numerical optimisation algorithm.

1) Objective function: The cost of transport is a measure of efficiency at a certain velocity allowing comparison between horizontal transportation modes and transportation of animals [19]. To quantify the price of speed [19], it is the work done normalised by the distance Δy travelled and the weight of the system. For pure vertical transportation,

TABLE II: Model parameters

Parameter	Symbol	Value
Total mass	m_0	9.1×10^{-3} kg
Mass body	$m_\mathrm{b} = 0.75 m_0$	6.8×10^{-3} kg
Mass leg	$m_\mathrm{leg} = 0.1 m_0$	9.1×10^{-4} kg
Mass tail	$m_\mathrm{tail} = 0.05 m_0$	4.55×10^{-3} kg
Moment of inertia body	$j_\mathrm{b} = 1/5 m_\mathrm{b}(a^2 + b^2)$	3.74×10^{-7} kg m^{-2}
Moment of inertia leg	$j_\mathrm{leg} = 1/12 m_\mathrm{leg} l_\mathrm{leg}^2$	7.58×10^{-9} kg m^{-2}
Moment of inertia tail	$j_\mathrm{tail} = 1/12 m_\mathrm{tail} l_\mathrm{tail}^2$	6.06×10^{-8} kg m^{-2}
Length leg	l_leg	1×10^{-2} m
Length tail	l_tail	4×10^{-2} m
Length body semi-axis	a	7×10^{-3} m
Length body semi-axis	b	15×10^{-3} m
Max torque	τ_max	2.3×10^{-1} N m^{-1}
Damping	r	1×10^{-4} N s m^{-1} rad^{-1}
Max power	P_max	0.5 W
Max horizontal force tail	$\lambda_{\mathrm{tail},x}$	$\geq 1 \times 10^{-6}$ N

this cost of transport can also have another interpretation in climbing transport, it is the energy put into the system over the energy gained by height Δy

$$C_\mathrm{CoT} = \frac{W}{mg\Delta y} \tag{15}$$

The absolute mechanical work done summed over all actuators is given by integrating the torque of the actuator times the joint velocity of the actuator

$$W = \int_{t_0}^{t_\mathrm{end}} \sum_{i=\mathrm{A,B,C}} |\tau_i \dot{\mathbf{q}}_i| \mathrm{d}t \tag{16}$$

2) Control: The control inputs $\tau_i(t)$ are an open-loop excitation law as a function of time comparable to the spinal reflexes found in animals [36]. Closed loop control law, inputs dependent on states $\tau((\dot{\mathbf{q}}), \mathbf{q}, t)$, is not considered because it would unnecessarily complicate the control action. The open-loop excitation is parameterised as a piece-wise constant function. Other parameterizations defining the excitation function like the coefficient of polynomials, splines, Taylor series or Fourier series all constrain the system.

3) Discretisation: The discretisation of the optimisation can be implemented in different ways. For the same reasoning as [37] (see appendix), we choose to use a direct orthogonal collocation method for discretisation.

With direct collocation, constraint violations can be expressed analytically. Intermediate states are defined by a polynomial of degree d, which ensures that the solution is smooth. At the bounds of segments, continuity is enforced. Increasing accuracy is achieved by either increasing the number of segments or the order of the polynomial [38]. A third degree polynomial $d = 3$ is chosen, such that the state $\mathbf{q}$ can be accurately estimated with a constant control input $\mathbf{u}$. Differentiating a constant twice results in a cubic function.

Solving a multi-phase problem can be considered as solving multiple single-phase problems in parallel. The key difference is that the boundary constraints between any two phases can be connected, thus coupling the trajectory segments.

Total trajectory exists of N stages, the n-th stage is divided into $M(n)$ segments. Considering 3 stages, stage 1 as the contact stage to accelerate upwards eq. (6), at lift off the contact forces become zero. Entering stage 2, the free-flying stage, the equation of motion is eq. (7). At reattachment, there is a plastic collision given by eq. (14), followed by stage 3, which is contact again eq. (6).

For the n-th stage the time step is $h(n)$. The time steps $h(n)$ is a decision variable of the optimisation problem to allow the stage transitions to take place in a time period. The total time of one stride is constrained to the time steps multiplied by the number of segments $\Delta t = \sum_n h(n) M(n)$. For all stages we choose to use ten segments $M(n) = 10$. For details and illustrations see appendix.

The objective function has discontinuous derivatives because of the absolute value function. In this case the absolute work done by actuators $|\tau_i \dot{\mathbf{q}}_i|$. This discontinuity can be bypassed by rewriting the objective function with slack variables [38], expressing the absolute terms in positive s^+ and negative s^- components and constrain these components to be positive and the positive minus the negative equal to the work.

$$\begin{aligned} \min |\tau_i \dot{\mathbf{q}}_i| \quad \rightarrow \quad & \min && s_i^+ + s_i^- \\ & \text{subject to} && s_i^+ - s_i^- = \tau_i \dot{\mathbf{q}}_i \\ & && s_i^+ \geq 0 \\ & && s_i^- \geq 0 \end{aligned} \tag{17}$$

Introducing slack variables requires more decision variables, consequently increasing optimisation time, but without losing accuracy. Where this would be the case if an approximation is used for the absolute value function.

With this, we can set up a search for an optimal motion for a minimal objective function C to be a constraint nonlinear optimisation problem

$$\begin{aligned} &\min(C) \\ &h_1, \ldots, h_n, \mathbf{q}_1, \ldots, \mathbf{q}_N, \dot{\mathbf{q}}_1, \ldots, \dot{\mathbf{q}}_N, \\ &\tau_1 \ldots \tau_N, \mathbf{s}_1, \ldots, \mathbf{s}_N \end{aligned} \tag{18}$$

where states $\mathbf{q}$, $\dot{\mathbf{q}}$ are subject to equality constraints on the equation of motion of eq. 6, eq. 7 depending on the stage.

4) Constraints: Besides that in the optimisation the decision variables are constrained by the system dynamics in an equality constraint, they are also equality constraint by the initial and end position. The initial position $\mathbf{q}_1$ is set approximately the same as the initial position of the treecreeper of Norberg. The initial position and final position are constrained to be exactly the same plus a jump height. The initial and final velocities are constrained to zero $\dot{\mathbf{q}} = 0$.

During the flying stage, the contact point of the foot and the tail are constrained to not go through the vertical surface, i.e. the position should be positive because the vertical surface is located at $x = 0$.

Futhermore, the decision variable τ are constraint by maximal torque τ_max and the power, described by slack variable $\mathbf{s}$, is constraint to maximal power P_max (tab. II).

The optimisation is implemented in MATLAB calling the open-source nonlinear optimisation tool CasADi [39]. For solving the problem an open-source primal-dual interior point method solver is used, IPOPT [40]. For the solver, a maximum number of 2000 iterations is set.

D. Variations

To investigate the influence of parameters and objective function on the dynamics of climbing we will vary them. First, we will study the results for one set of parameters, the nominal parameters. These parameters are based on the parameters of treecreeper [6]. The jump height and jump time will be set to the jump height $\Delta y = 66\,\text{mm}$ and jump time $\Delta t = 0.1375\,\text{s}$ reported by Norberg [6]. We will present the results of the work done by the individual actuators and the potential energy gained.

1) Jump height: To investigate if the cost of transport is dependent on jump height and if there is an optimal climbing height given the model and parameters, the jump height is varied.

2) Damping variation: The system is not conservative due to damping. If there would be no damping/dissipation, all trajectories would have the same cost. We will investigate the role of the damping by varying it.

3) Variation objective function: The objective function will be extended to take into account thermal loss due to static holding torque. In robotic and biological systems the generation of mechanical work is accompanied by additional thermal losses. For example, with static force, with no mechanical flow but with mechanical effort, there is energy lost to the thermal domain. To take this into account, an additional term P_{loss} is introduced in the objective function. Torque relates linearly to current $\tau \propto i$, for DC motors heat loss relates quadratic with current $P_{\text{loss}} = (1/R)i^2$ resulting in cost/objective function

$$\begin{aligned} C_{\text{CoT}+\tau^2} &= \text{CoT} + E_{\text{loss}} \\ &= \text{CoT} + \frac{1}{R}\int_{t_0}^{t_{\text{end}}} \sum_{i=\text{A,B,C}} \tau_i^2 \mathrm{d}t \end{aligned} \tag{19}$$

E. Modified model: Without tail

To investigate what the benefits are of tail support, we create a model without a tail. Without the tail and only actuators at the hip and the knee the model will not be able to climb. An additional actuator is required at the ankle. Until now we assumed that the ankle joint was not actuated and was without damping, in other words a free hinge point. The model is adjusted accordingly. Let us consider the ankle joint angle α_{D}, and torque τ_{D}, then the states become,

$$\mathbf{q} = \begin{bmatrix} x & y & \varphi & \alpha_{\text{A}} & \alpha_{\text{B}} & \alpha_{\text{D}} \end{bmatrix} \tag{20}$$

and the control wrench becomes

$$\mathbf{u} = \begin{bmatrix} 0 & 0 & 0 & \tau_{\text{A}} & \tau_{\text{B}} & \tau_{\text{D}} \end{bmatrix} - \mathbf{d}\dot{\mathbf{q}} \tag{21}$$

where damping $\mathbf{d}$ is chosen the same as for all other joints as described in eq. 5.

The foot is now modelled as a body with mass and inertia. For convenience, these parameters are chosen equal to the mass and inertia of the tail. The rigid body of the foot is not allowed to translate and rotate, yielding the contact constraint can be described by

$$\dot{\mathbf{r}} = \begin{bmatrix} \dot{x}_{\text{foot}} \\ \dot{y}_{\text{foot}} \\ \dot{\alpha}_{\text{foot}} \end{bmatrix} = 0. \tag{22}$$

With this, the contact wrench is $\lambda = \begin{bmatrix} \lambda_{\text{foot},x}, & \lambda_{\text{foot},y}, & \lambda_{\text{foot},\alpha} \end{bmatrix}$.

The equation of motion of this modified model is described with the same method as in previous sections, with the impact and contact force expressions.

III. Results

The next section is structured as follows. First, the results of the video data are presented. Second, the results of the optimisation are presented.

A. Results nature - video

In fig. 3 the positions and orientations are shown for all 13 jumps of the 8 individual birds normalised with jump height and set out against relative time. The grey lines indicate the individual jumps. The red line indicates the trajectory of the treecreeper of Norberg [6]. The blue line is the average of the position and orientation of all the birds (grey and red lines). The x-position all start at 0.2 for illustration purposes, such that the surface is located at $x = 0$. All birds move towards (fig. 3 b1) the trunk in the initial phase of the stride. The final y position of all birds is equal to one since all are normalised by their jump height. All rotate (fig. 3 b3) in the positive direction (counterclockwise) with the head towards the trunk with the average peaking at 15°. The floating phase, the phase where the bird does not have contact with the surface, starts on average at 52 % of total time, and ends at 81 %. We observed that the tail is lifted off the bark before the feet in all videos. After the floating phase, the feet and tail make contact with the bark at approximately the same time. In sub-figure b4) the time without contact is determined by the feet not having contact with the tree trunk.

In fig. 4 the stride height is shown against jump time for all 13 jumps. The error bars in the x direction indicate the video's frame rate. The error bar in the y direction indicates the range in the length scaling. The length of the bird species is reported as a range, see tab. I. The error bar in the horizontal direction for the spotted woodpecker in orange is small (1/400 Hz) as that one is captured with the high-speed camera resulting in more accuracy regarding positions in time. It can be observed that all measurements fall within the ballistic limit. The pileated woodpecker 1 is the fastest with a velocity of $1.4\,\text{m}\,\text{s}^{-1}$ in the videos considered.

B. Results optimisation

The results of the optimisation will be presented in this section. First work done per actuator is shown for a fixed stride height and stride time for the nominal parameters.

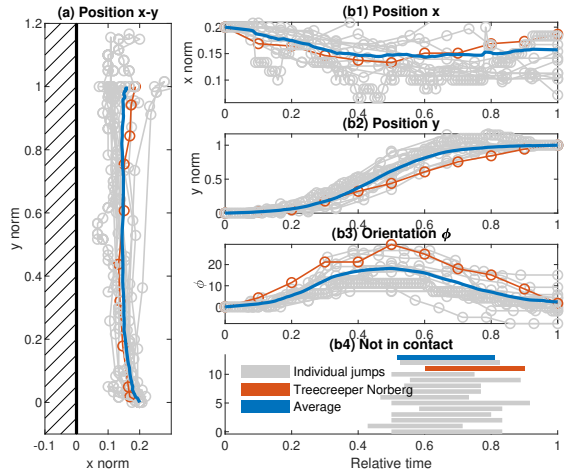

Fig. 3: Processed bird video data: (a) Position x against y normalised by jump height. (b1) position x normalised by jump height against relative time (b2) position y normalised by jump height against relative time (b3) orientation φ against relative time. (b4) Time without contact. All 13 jumps are grey lines (of 8 individual birds), average is the blue line, treecreeper of Norberg [6] is red line.

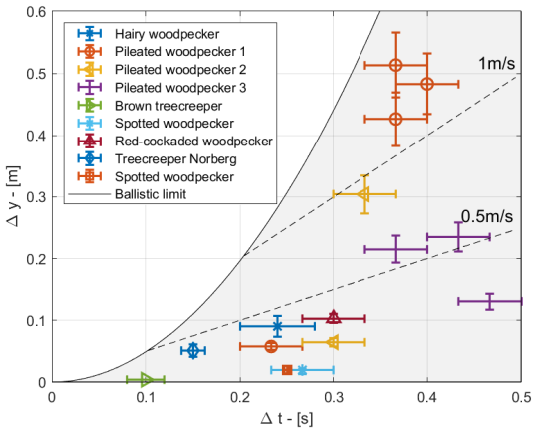

Fig. 4: Processed bird video data: Jump height Δy in m against jump time Δt in s for individual birds some with multiple jumps, with ballistic limit given by $y_{max} = 1/2(gt^2_{max})$, where error bars in x direction indicate fps and error bars in y direction range of length scaling, see tab. I.

Followed by solutions for variation of damping. Next, the results of jump height variations are shown. The result of the modified objective function is presented. Finally, the result of the modified model is shown. Note that throughout the presented results the trajectory of the nominal solution is always shown with a dark blue solid line and the trajectory of the treecreeper (of Norberg [6]) is always shown with a red line with markers. Specifically, the treecreeper trajectory is shown because the parameters for the model are based on the treecreeper.

For nominal parameters and objective function, the trajectory, kinetic and potential energy, and work done per actuator are shown in fig. 5. On the right side the total work of all actuators, work done per actuator and the gained potential energy are shown against time. The shaded area indicates the time the model is not in contact with the surface, i.e. the model is free-flying. In the first phase, the actuators A (hip) and C (tail) are delivering most of the mechanical work. This work is partly stored in the kinetic and the potential energy and partly dissipated in the damping. The actuator B is not delivering work in the first phase, since the angle α_B is not changing, but actuator B is delivering torque in this phase. However, just before the lift-off, actuator B is delivering work. Just after the lift-off, all actuators are delivering work. This work is mostly dissipated in the damping. At the start of the flying phase, the lower leg is pulled towards the main body, thereby the model gains kinetic energy. During the flying phase, there is a gradual increase in potential energy and a gradual decrease in kinetic energy. The power per actuator for the first phase is reaching the maximal power constraint P_{max}. The torques required for this solution are not approaching the maximal torque constraint τ_{max}.

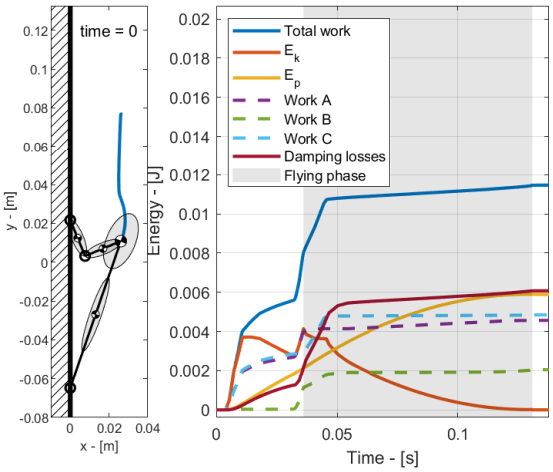

Fig. 5: Results of optimisation: Left figure is the trajectory shown, right figure is the work done per actuator shown (A is hip joint, B is knee joint, C is tail joint (fig. 2)) for jump height $\Delta y = 66\,\text{mm}$ with total time of $\Delta t = 0.1375\,\text{s}$

The results of the effect of the damping on the optimal trajectory are shown next. The optimal solution for varying damping for jump height $\Delta y = 66\,\text{mm}$ with a total time of $\Delta t = 0.1375\,\text{s}$ is shown in fig. 6. The positions (x, y) and the orientations (φ) of the main body are displayed. In subfigure (a), the positions (x, y) are displayed, with the model visualised for the initial position. For larger damping than $r = 2 \times 10^{-4}\,\text{N s m}^{-1}\,\text{rad}^{-1}$ the optimisation converges to an infeasible solution, there can not be enough power delivered due to power constraints on the actuators. The dark blue line indicates the trajectory for the nominal parameters, which is corresponding to the energies and work plotted in fig. 5. The position of the main body rotates around the foot contact point in the first phase for the nominal damping solution.

The lift-off position in x direction is slightly (1 mm) smaller compared to the initial position. For a larger damping value, the trajectory is almost identical. For a smaller damping value, the x position of the main body is deviating less from its initial position. The x positions of the optimisation are initially away from the surface and then towards the surface, where the Treecreeper is directly moving towards the surface. The lift-off position in x direction of the Treecreeper is 40 mm closer to the surface compared to the initial position.

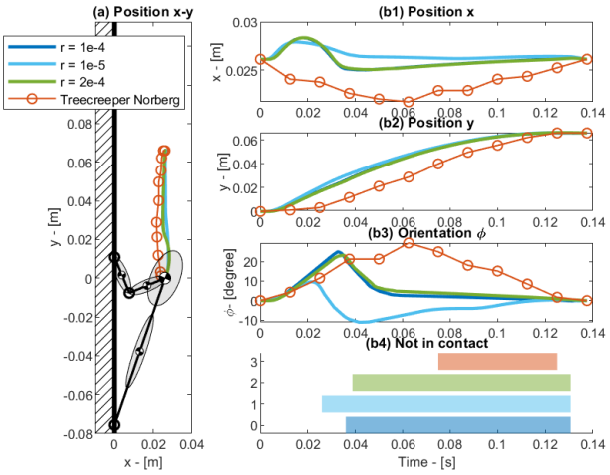

Fig. 6: Results of optimisation: Varying damping for jump height $\Delta y = 66$ mm and total time $\Delta t = 0.1375$ s. Blue lines are nominal case damping, red lines are less damping, yellow lines are more damping, purple lines are Norberg Treecreeper [6] positions. Position (x, y) and orientation φ of main body (a) position x vs y, (b1) x position, (b2) y position, (b3) orientation angle φ and (b4) time without contact.

The percentage of work done by actuators A (hip joint), B (knee joint) and C (tail joint) of the total work done at the end of the stride for the various damping values is given in tab. III. One could observe a trend that for an increase in damping the actuator B has to deliver more work. The cost of transport for the solutions is also shown in the table. The cost of transport increases for a large damping value and vice versa.

The results for a range of jump height Δy for fixed total time $\Delta t = 0.14$ s are shown in fig. 7. All the trajectories, kinetic and potential energy, and work done per actuator are shown in fig. 7a. The data is all plotted in one plot to show that the optimisation finds approximately the same solution. The cost of transport given the jump height is shown in fig. 7b. For the given jump heights the minimal cost of transport is at $\Delta y = 83$ mm. For jump heights of $\Delta y = 98$ mm, the solver cannot find a feasible solution within 2000 iterations. The ballistic limit, given the jump time $\Delta t = 0.14$ s, is at a jump height of $\Delta y_{\max} = 96.1$ mm.

In fig. 8 the trajectories are shown for objective function cost of transport C_{CoT} and cost of transport summed with torque squared $C_{\mathrm{CoT}+\tau^2}$ of eq. 19 with a weight factor 10000 ($R = 1 \times 10^{-4}$). The resulting cost of transport is given in tab.

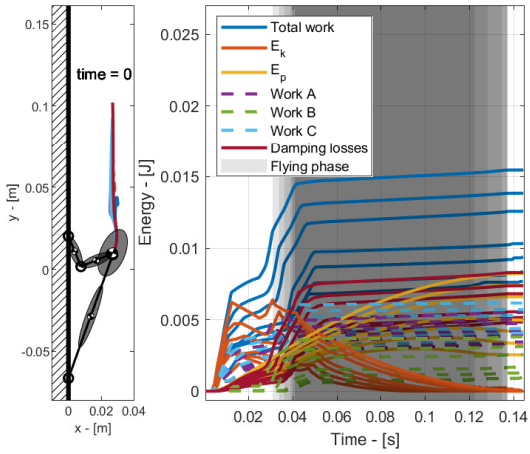

(a) Left figure are the trajectories shown, right figure is the work done per actuator shown

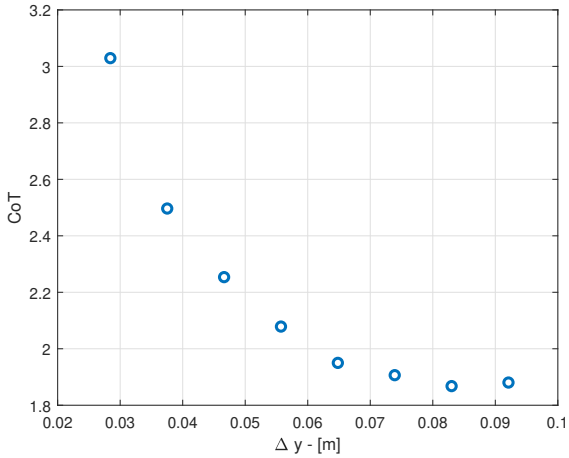

(b) Cost of transport (CoT) against jump height Δy

Fig. 7: Results of optimisation: Varying of jump height Δy for fixed total time $\Delta t = 0.14$ s, the ballistic limit here is $\Delta y_{\max} = 0.0961$ m

III. The cost of transport is 1.5 times larger for the modified objective function than for the unmodified one. The main body moves towards the surface for this modified objective function $C_{\mathrm{CoT}+\tau}$ during the first phase, whereas this is not the case for the unmodified one C_{CoT}. The peak torque over all actuators for the cost of transport as objective function is 0.0408 N m and for the modified objective function is 0.0093 N m.

a) Modified model: Without tail: The trajectories of the modified model without a tail but with actuated ankle are shown in fig. 9 indicated with yellow lines. The objective function used to find the trajectory for this modified model is the cost of transport C_{CoT}. The main body moves towards the surface directly. The lift-off position in x is 6 mm closer to the surface than the initial position. The orientation of the main body decreases more gradually than for the model with a tail.

The work done per actuator and the cost of transport is

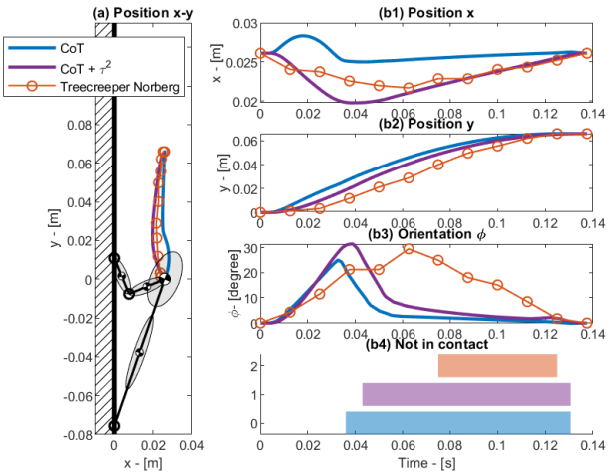

Fig. 8: Results of optimisation: For objective function $C_{\mathrm{CoT}+\tau}$ (torque squared) eq. 19) left figure is the trajectory shown, right figure is the work done per actuator shown (A is hip joint, B is knee joint, C is tail joint (fig. 2)) for jump height $\Delta y = 66\,\mathrm{mm}$ with total time of $\Delta t = 0.1375\,\mathrm{s}$.

shown in tab. III. The cost of transport for this modified model without a tail is approximately 2 times larger than for the nominal model with a tail. More than half of the total work for the modified model is done by the actuator D (ankle joint).

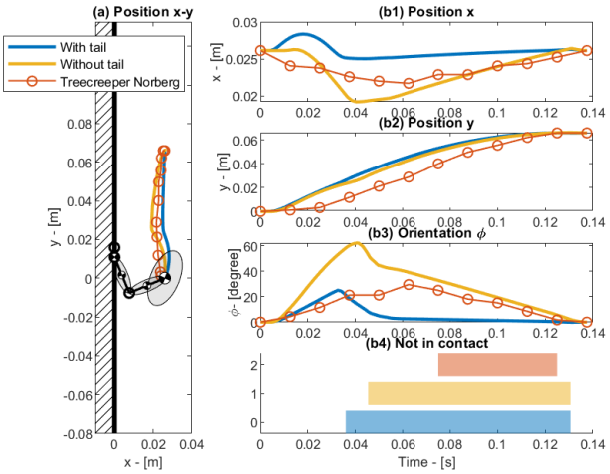

Fig. 9: Results of optimisation: Without tail, but with ankle for jump height $\Delta y = 66\,\mathrm{mm}$ with total time of $\Delta t = 0.1375\,\mathrm{s}$.

IV. Discussion

In the following section, we will discuss the trajectories for the variations of the optimisation and compare them with the trajectory of the treecreeper.

A. Trajectories/gait

1) Positions: In nature, the main body of all the birds moves closer to the tree (fig. 3 b1) in the initial phase of the movement. One reason for this could be to shorten the lever arm from the contact point to the hip joint, implying that the (muscular) torque about the hip joint can be reduced for the same force on the surface $\tau = \ell \times F$. Another reason for moving closer could be to have some margin for reattachment. Such that the tree is well in reach of the feet for reattachment. Or to allow the bird to push slightly away from the tree before a full standstill. It could also be that the bird moves closer to the tree to realise a longer path over which the muscles can exert a force while in contact with the surface.

For the model with nominal parameters and cost of transport as objective function fig. 5 the main body rotates around the foot as a hinge point, gaining kinetic energy in the first phase of the stride. Next, the main body flies freely only vertically upwards. This gait/trajectory is expected since keeping the knee joint B almost static saves mechanical work. Most actuator work is done in the first stage of the stride, which is expected since the robotic model should accelerate sufficiently to fly and reattach again.

By taking into account the static holding torque, in this case adding the torque squared in the objective function fig. 8 resulted in a trajectory that is more comparable to that one of the treecreeper, by slipping closer to the trunk in the first phase of the stride. The modified objective function lays a cost on the delivered torques. This better matching trajectory between the model with the modified objective function and treecreeper could mean that for the nominal objective function, the model is generating unnatural torques. This trajectory required more mechanical work (tab. III) than the trajectory optimised for only the cost of transport. This could be caused by that the total torque is less but acting over a longer time period and thereby delivering more mechanical work.

2) Orientation: Besides all birds moving towards the tree, all birds perform a rotation of the body with respect to the initial orientation in the positive direction (head towards the tree) fig. 3 b2) in initial part of stride. A reason for this could be to counteract the backward pitch caused by the torque on the hip joint moving the legs backwards relative to the body.

For the model for both objective functions, the main body also rotates in the positive direction in the first phase. The maximal orientation angle is approximately the same as the treecreeper. The model starts rotating in backward direction after lift-off, this applies to the treecreeper. Both are rotating backwards in the flight phase. There is a difference in the progression of the orientation in time. The orientation of the model decreases faster after lift-off. The treecreeper rotates backwards more gradually. The models shows sharp negative rotation because the actuator A (hip joint) is producing large positive torque.

3) Contact time/phases: The time without contact (flying phase) is longer for the model 72 % than for the treecreeper 36 %. A shorter flying phase implies that feet need to be displaced faster to the new contact point. A shorter acceleration phase implies that the main body needs faster acceleration, such that enough kinetic energy is stored to

TABLE III: Results optimisation for variations for fixed $\Delta y = 66\,\text{mm}$ and total time $\Delta t = 0.1375\,\text{s}$

	Variation damping fig.6			**Variation objective** fig.8	**Variation model** fig.9
		Nominal			
Damping r [$\text{Nsm}^{-1}\text{rad}^{-1}$]	$r = 1 \times 10^{-5}$	$r = 1 \times 10^{-4}$	$r = 2 \times 10^{-4}$	$r = 1 \times 10^{-4}$	$r = 1 \times 10^{-4}$
Objective function	C_{CoT}	C_{CoT}	C_{CoT}	$C_{CoT+\tau^2}$	C_{CoT}
Model	With tail	With tail	With tail	With tail	Without tail
Work done by actuator A	52 %	40 %	39 %	40 %	10 %
Work done by actuator B	14 %	18 %	27 %	23 %	36 %
Work done by actuator C or D	34 %	42 %	34 %	37 %	54 %
CoT	1.95	1.53	2.81	2.42	3.15

travel the vertical distance. Faster acceleration requires larger maximal power because in a shorter time the system requires the same amount of energy.

B. Damping

The trajectory is determined by the unconservative model due to damping at the joints. For smaller damping than the nominal damping, the trajectory is slightly different but has the same characteristic, of rotating around the foot contact. For larger damping, the trajectory is almost identical. A reason for the same trajectory could be that the damping is modelled in parallel with the actuator. Yielding that scaling the damping would only scale the torques required. But it could also be that the optimisation solver finds another local minimum solution due to numerical inaccuracy.

We neglected the resistance between the tail tip and the surface. This could influence the results, since having a resistance at the tail tip would penalise the movement of tail tip over the surface.

Another dissipative element we neglected is air drag. Air drag increases quadratically with velocity. For small velocities, the drag would be neglectable. However, for larger velocities, it would be larger and dissipate more energy. This could influence the optimal climbing velocity, by shifting the optimal climbing velocity down.

C. Energetic behaviour

The kinetic energy summed over all rigid bodies (orange line fig. 5) increases initially, decreases and increases again before lift-off. The increase in the sum of kinetic energies just before lift-off is mainly caused by an increase in the translational kinetic energy of the mass of the lower leg. This energy increases due to an increase in velocity.

During the free-flying phase, the kinetic energy decreases quadratically, which is as expected for a free-flying object.

D. Jump height & Optimal velocity

The larger and heavier birds tend to jump higher and faster than the smaller lighter birds as can be seen in fig. 4. The larger birds are faster climbers than the smaller birds by looking at individual jumps. A reason for this could be that the larger and heavier birds have more powerful muscles allowing faster acceleration, thus more velocity.

The pileated woodpecker 3 in fig. 4 jump consecutively lower and slower than pileated woodpecker 1. This illustrates the argument that the bird is choosing stride length and stride time, hence velocity, given a task.

For variations in jump height Δy in fig. 7 the cost of transport decreases for an increase in jump height and because the jump time Δt is fixed, an increase in velocity. In other words, it is more efficient to jump higher. The reason for this can be seen in fig. 7a, for the jumps with less height gain, the main body overshoots the height, i.e. first falls down a small bit before reattachment. In fig. 7a it can be seen that the higher the jump is, the higher the total work required is. The trajectories are for the first stage approximately the same, for all jump heights, the main body is rotating around the foot contact point.

E. Model

For the model without a tail, but with an actuated ankle, we can see that the trajectory is different from the one with a tail. Both with the cost of transport as the objective function. The main body moves towards the surface, and the lift-off x-position is closer to the surface than the initial position. The reason for this could be that the torque required at the ankle joint D is reduced when the lever arm to the main body decreases. This could suggest that the tail of the bird is not as powerful as the other joints.

The power delivered by joint D is prominent as expected because there is no tail meaning that the main body is predominately lifted by the ankle joint.

The not entirely matching trajectory between the model and the birds can have various reasons. The muscles are modelled as pure torque actuators with torque and power constraints, however, this may be oversimplified. For example, positive muscle work is considered cheaper than negative work [6]. Another reason for the mismatch could be that the torque bandwidth is unlimited, allowing an infinite change in torque. Furthermore, the mismatch could be caused by allowing unlimited contact force for the foot. The foot is allowed to pull and push on the surface with unlimited force. However, the contact force of a claw with a surface is limited [41]. This could influence the trajectory. Also, the mismatch in trajectory could be coming from the kinematic relations. The joint location with both the tail and hip joint at the same location may not be representable for the birds. Having the joints located in the body at a different location would change the kinematic relations and therefore change the dynamics.

V. CONCLUSION

To study tail-supported climbing, videos of birds are analysed, a model is created and the optimal trajectories are

determined by minimising an objective function. The kinematic gait (trajectory) of the climbing birds is comparable for a variety of species with different masses and dimensions. The larger and heavier birds tend to have a higher climbing velocity because they jump higher. The trajectory of the model for minimal mechanical work is not matching with the trajectories of the birds. This work shows that for the specific assumptions and parameters tail supported climbing without actuated ankle joint has a better cost of transport than without tail but with actuated ankle joint. This indicates that tail-supported climbing could be more efficient.

This research shows that tail-supported climbing is relevant for the dynamic case and that it would be very interesting to do future research.

In future work, it would be beneficial to measure the contact forces of the birds. For the model it would be interesting to displace the location of joints within the body. Also, it would be interesting to constrain the contact force and/or implement a claw contact model. Furthermore, it would be valuable to investigate the influence of introducing a fourth phase where only the foot is in contact with the surface and already tail is lost contact. Moreover, it would be suited to create a prototype to validate the model and optimisation. Additionally, it would be relevant to investigate the influence of the scaling of dimensions and mass with climbing velocity, because the larger/heavier birds jump with higher velocity.

VI. Acknowledgement

Firstly, I would like to thank ir. A. Dijkshoorn, ir. R. Sneep and prof.dr.ir. G. Krijnen for their continued feedback and excellent guidance during the thesis process. Their experience has helped to guide the research more effectively and their critical thinking always provided useful feedback.

Secondly, I would like to thank the Macaulay Library at the Cornell Lab of Ornithology for allowing us to use their videos of climbing birds.

References

[1] D. Floreano and R. J. Wood, "Science, technology and the future of small autonomous drones," *nature*, vol. 521, no. 7553, pp. 460–466, 2015.

[2] K. Karydis and V. Kumar, "Energetics in robotic flight at small scales," *Interface focus*, vol. 7, no. 1, p. 20160088, 2017.

[3] W. R. Roderick, M. R. Cutkosky, and D. Lentink, "Touchdown to take-off: at the interface of flight and surface locomotion," *Interface focus*, vol. 7, no. 1, p. 20160094, 2017.

[4] F. Richardson, *Adaptive modifications for tree-trunk foraging in birds*. University of California Press, 1942, vol. 46.

[5] H. Winkler and W. J. Bock, "Analyse der kräfteverhältnisse bei klettervögeln," *Journal für Ornithologie*, vol. 117, no. 4, pp. 397–418, 1976.

[6] R. Å. Norberg, "Treecreeper climbing; mechanics, energetics, and structural adaptations," *Ornis Scandinavica*, pp. 191–209, 1986.

[7] A. Daanje, "On locomotory movements in birds and the intention movements derived from them," *Behaviour*, pp. 48–98, 1950.

[8] J. E. Law, "Down-tree progress of sitta pygmaea," *The Condor*, vol. 31, no. 2, pp. 45–51, 1929.

[9] M. Fujita, K. Kawakami, S. Moriguchi, and H. Higuchi, "Locomotion of the eurasian nuthatch on vertical and horizontal substrates," *Journal of Zoology*, vol. 274, no. 4, pp. 357–366, 2008.

[10] L. W. Spring, "Climbing and pecking adaptations in some north american woodpeckers," *The Condor*, vol. 67, no. 6, pp. 457–488, 1965.

[11] R. J. Raikow, "Structure and variation in the hindlimb musculature of the woodcreepers (aves: Passeriformes: Dendrocolaptinae)," *Zoological Journal of the Linnean Society*, vol. 107, no. 4, pp. 353–399, 1993.

[12] A. Hajeer, L. Chen, and E. Hu, "Review of classification for wall climbing robots for industrial inspection applications," in *2020 IEEE 16th International Conference on Automation Science and Engineering (CASE)*. IEEE, 2020, pp. 1421–1426.

[13] M. T. Pope, C. W. Kimes, H. Jiang, E. W. Hawkes, M. A. Estrada, C. F. Kerst, W. R. Roderick, A. K. Han, D. L. Christensen, and M. R. Cutkosky, "A multimodal robot for perching and climbing on vertical outdoor surfaces," *IEEE Transactions on Robotics*, vol. 33, no. 1, pp. 38–48, 2016.

[14] A. Ji, Z. Zhao, P. Manoonpong, W. Wang, G. Chen, and Z. Dai, "A bio-inspired climbing robot with flexible pads and claws," *Journal of Bionic Engineering*, vol. 15, no. 2, pp. 368–378, 2018.

[15] A. Saunders, D. I. Goldman, R. J. Full, and M. Buehler, "The rise climbing robot: body and leg design," in *Unmanned Systems Technology VIII*, vol. 6230. International Society for Optics and Photonics, 2006, p. 623017.

[16] M. A. Estrada, E. W. Hawkes, D. L. Christensen, and M. R. Cutkosky, "Perching and vertical climbing: Design of a multimodal robot," in *2014 IEEE international conference on robotics and automation (ICRA)*. IEEE, 2014, pp. 4215–4221.

[17] G. A. Lynch, J. E. Clark, P.-C. Lin, and D. E. Koditschek, "A bioinspired dynamical vertical climbing robot," *The International Journal of Robotics Research*, vol. 31, no. 8, pp. 974–996, 2012.

[18] W. R. Provancher, S. I. Jensen-Segal, and M. A. Fehlberg, "Rocr: An energy-efficient dynamic wall-climbing robot," *IEEE/ASME Transactions on Mechatronics*, vol. 16, no. 5, pp. 897–906, 2010.

[19] T. v. K. G. Gabrielli, "What price speed? specific power required for propulsion of vehicles," *Journal of the American Society for Naval Engineers*, vol. 63, no. 1, pp. 188–200, 1951.

[20] W. Xi, Y. Yesilevskiy, and C. D. Remy, "Selecting gaits for economical locomotion of legged robots," *The International Journal of Robotics Research*, vol. 35, no. 9, pp. 1140–1154, 2016.

[21] H. J. Ralston, "Energy-speed relation and optimal speed during level walking," *Internationale Zeitschrift für Angewandte Physiologie Einschliesslich Arbeitsphysiologie*, vol. 17, no. 4, pp. 277–283, 1958.

[22] B. R. Umberger and P. E. Martin, "Mechanical power and efficiency of level walking with different stride rates," *Journal of Experimental Biology*, vol. 210, no. 18, pp. 3255–3265, 2007.

[23] N. Pistorius. Spotted woodpecker captured at 400hz. Youtube. [Online]. Available: https://youtube.com/shorts/1YFbgDojeoE?feature=share

[24] P. de Groot Boersma. Hairy woodpecker (rocky mts.). macaulaylibrary. [Online]. Available: https://macaulaylibrary.org/asset/200882831

[25] Hairy woodpecker identification. TheCornellLab. [Online]. Available: https://www.allaboutbirds.org/guide/Hairy_Woodpecker/id

[26] M. Husbands. Pileated woodpecker visit this morning. Youtube. [Online]. Available: https://www.youtube.com/watch?v=0_n1pb2Mr98&ab_channel=MarkHusbands

[27] Pileated woodpecker identification. TheCornellLab. [Online]. Available: https://www.allaboutbirds.org/guide/Pileated_Woodpecker/id

[28] T. Barksdale. Pileated woodpecker. macaulaylibrary. [Online]. Available: https://macaulaylibrary.org/asset/442357#_ga=2.74038615.415197061.1647688424-1394849067.1647688424

[29] W. M. Birding. Pileated woodpecker climbing and investigating. Youtube. [Online]. Available: https://www.youtube.com/watch?v=0_n1pb2Mr98&ab_channel=MarkHusbands

[30] WatchRWildlife. Tree creeper 10-10-2017. Youtube. [Online]. Available: https://www.youtube.com/watch?v=rEsq8UURU8U&ab_channel=WatchRWildlife

[31] Brown creeper identification. TheCornellLab. [Online]. Available: https://www.allaboutbirds.org/guide/Brown_Creeper/id

[32] Brown creeper identification. TheCornellLab. [Online]. Available: https://www.birdspot.co.uk/bird-identification/great-spotted-woodpecker

[33] J. Shi *et al.*, "Good features to track," in *1994 Proceedings of IEEE conference on computer vision and pattern recognition*. IEEE, 1994, pp. 593–600.

[34] G. Folkertsma, "Energy-based and biomimetic robotics," *Ph.D. Thesis*, no. 5590, 2017.
[35] D. W. Haldane, M. M. Plecnik, J. K. Yim, and R. S. Fearing, "Robotic vertical jumping agility via series-elastic power modulation," *Science Robotics*, vol. 1, no. 1, 2016.
[36] T. G. Brown, "Studies in the physiology of the nervous system. viii. neural balance and reflex reversal, with a note on progression in the decerebrate guinea-pig," *Quarterly Journal of Experimental Physiology: Translation and Integration*, vol. 4, no. 3, pp. 273–288, 1911.
[37] C. D. Remy, K. Buffinton, and R. Siegwart, "A matlab framework for efficient gait creation," in *2011 IEEE/RSJ International Conference on Intelligent Robots and Systems*. IEEE, 2011, pp. 190–196.
[38] J. T. Betts, *Practical methods for optimal control and estimation using nonlinear programming*. SIAM, 2010.
[39] J. A. E. Andersson, J. Gillis, G. Horn, J. B. Rawlings, and M. Diehl, "CasADi – A software framework for nonlinear optimization and optimal control," *Mathematical Programming Computation*, vol. 11, no. 1, pp. 1–36, 2019.
[40] L. T. Biegler, *Nonlinear programming: concepts, algorithms, and applications to chemical processes*. SIAM, 2010.
[41] W. R. Roderick, H. Jiang, S. Wang, D. Lentink, and M. R. Cutkosky, "Bioinspired grippers for natural curved surface perching," in *Conference on Biomimetic and Biohybrid Systems*. Springer, 2017, pp. 604–610.
[42] M. Tavakoli and C. Viegas, "Bio-inspired climbing robots," in *Biomimetic Technologies*. Elsevier, 2015, pp. 301–320.
[43] W. R. Roderick, D. D. Chin, M. R. Cutkosky, and D. Lentink, "Birds land reliably on complex surfaces by adapting their foot-surface interactions upon contact," *Elife*, vol. 8, p. e46415, 2019.
[44] N. S. Proctor and P. J. Lynch, *Manual of ornithology: avian structure & function*. Yale University Press, 1993.
[45] A. Pike and D. Maitland, "Scaling of bird claws," *Journal of Zoology*, vol. 262, no. 1, pp. 73–81, 2004.
[46] M. Husbands. Pileated woodpecker visit this morning. Youtube. [Online]. Available: https://www.youtube.com/watch?v=0_n1pb2Mr98&ab_channel=MarkHusbands
[47] S. Kim, M. Spenko, S. Trujillo, B. Heyneman, D. Santos, and M. R. Cutkosky, "Smooth vertical surface climbing with directional adhesion," *IEEE Transactions on robotics*, vol. 24, no. 1, pp. 65–74, 2008.
[48] L. L. Reader, D. R. Carrier, F. Goller, M. R. Isaacs, A. Moore Crisp, C. J. Barnes, and D. V. Lee, "Climbing parrots achieve pitch stability using forces and free moments produced by axial–appendicular couples," *Journal of Experimental Biology*, vol. 225, no. 1, p. jeb242305, 2022.
[49] G. Gilardi and I. Sharf, "Literature survey of contact dynamics modelling," *Mechanism and machine theory*, vol. 37, no. 10, pp. 1213–1239, 2002.
[50] S. Kirchgeorg and S. Mintchev, "Hedgehog: Drone perching on tree branches with high-friction origami spines," *IEEE Robotics and Automation Letters*, vol. 7, no. 1, pp. 602–609, 2021.
[51] R. Alexander and H. Bennet-Clark, "Storage of elastic strain energy in muscle and other tissues," *Nature*, vol. 265, no. 5590, pp. 114–117, 1977.
[52] J. J. Videler, *Avian flight*. Oxford University Press, 2006.
[53] M. Kelly, "An introduction to trajectory optimization: How to do your own direct collocation," *SIAM Review*, vol. 59, no. 4, pp. 849–904, 2017.
[54] C. D. Remy, "Optimal exploitation of natural dynamics in legged locomotion," Ph.D. dissertation, ETH Zurich, 2011.
[55] M. Posa and R. Tedrake, "Direct trajectory optimization of rigid body dynamical systems through contact," in *Algorithmic foundations of robotics X*. Springer, 2013, pp. 527–542.
[56] A. Gosler, J. Greenwood, J. Baker, and N. Davidson, "The field determination of body size and condition in passerines: a report to the british ringing committee," *Bird Study*, vol. 45, no. 1, pp. 92–103, 1998.
[57] R. facts and motivation. woodpecker climbing on the tree-woodpecker shorts video- bird viral video- animals viral video. Youtube. [Online]. Available: https://www.youtube.com/watch?v=zmvQjlNU98M&ab_channel=RPfactsandmotivation
[58] A. Calgary. Woodpecker climbing trees in bowmont park. Youtube. [Online]. Available: https://www.youtube.com/watch?v=iTdWzFiqPf0&ab_channel=AdrianCalgary
[59] G. C. Haynes and D. E. Koditschek, "On the comparative analysis of locomotory systems with vertical travel," in *Experimental Robotics*. Springer, 2014, pp. 389–399.
[60] E. W. Hawkes, C. Xiao, R.-A. Peloquin, C. Keeley, M. R. Begley, M. T. Pope, and G. Niemeyer, "Engineered jumpers overcome biological limits via work multiplication," *Nature*, vol. 604, no. 7907, pp. 657–661, 2022.

A Model

This appendix covers the modelling background in more detail. The Euler-Lagrange formulation is used to obtain the equation of motion of the model. The model is a 2D planar model, with linear velocity in v_x and v_y and rotational velocity $!$.

The states of the model are defined by $\mathbf{q}$ and $\dot{\mathbf{q}}$. These states are kinematic relations between the rigid bodies. The linear velocity v_x and v_y and rotational velocity $!$ of the i-th rigid body are described as function of $\mathbf{q}$ and $\dot{\mathbf{q}}$.

A.1 Model Euler-Lagrange

The total kinetic energy of the system is equal to sum over the kinetic energies of all the rigid bodies

$$T = \frac{1}{2}\sum_i m_i(v_x^2 + v_y^2) + \frac{1}{2}\sum_i I_i\, !^2 \tag{A.1}$$

where the i-th rigid body has mass m_i and inertia I_i.

The total potential energy is equal to the sum of all potential energies of the rigid bodies

$$V = \sum_i m_i g y_i \tag{A.2}$$

where g is gravity and y_i the height of the rigid body.

The Lagrangian of the system is given by the total kinetic energy minus the total potential energy

$$\mathscr{L}(\dot{\mathbf{q}}, \mathbf{q}) = T - V \tag{A.3}$$

The Euler-Lagrange equation of motion is given by

$$\frac{\mathrm{d}}{\mathrm{d}t}\frac{\partial \mathscr{L}}{\partial \dot{\mathbf{q}}} - \frac{\partial \mathscr{L}}{\partial \mathbf{q}} = 0 \tag{A.4}$$

$$\frac{\partial}{\partial \dot{\mathbf{q}}}\frac{\partial \mathscr{L}}{\partial \dot{\mathbf{q}}}\ddot{\mathbf{q}} + \frac{\partial}{\partial \mathbf{q}}\frac{\partial \mathscr{L}}{\partial \dot{\mathbf{q}}}\dot{\mathbf{q}} - \frac{\partial \mathscr{L}}{\partial \mathbf{q}} = 0 \tag{A.5}$$

The mass matrix is expressed as

$$\mathbf{M}(\mathbf{q}) = \frac{\partial}{\partial \dot{\mathbf{q}}}\frac{\partial \mathscr{L}}{\partial \dot{\mathbf{q}}} \tag{A.6}$$

The Coriolis and gravitational forces are expressed as

$$\mathbf{f}_{\mathrm{cg}}(\dot{\mathbf{q}}, \mathbf{q}) = \frac{\partial \mathscr{L}}{\partial \mathbf{q}} - \frac{\partial}{\partial \mathbf{q}}\frac{\partial \mathscr{L}}{\partial \dot{\mathbf{q}}}\dot{\mathbf{q}} \tag{A.7}$$

The equation of motion can be expressed as

$$\mathbf{M}(\mathbf{q})\ddot{\mathbf{q}} = \mathbf{f}_{\mathrm{cg}}(\dot{\mathbf{q}}, \mathbf{q}) + \mathbf{u} \tag{A.8}$$

where $\mathbf{u}$ is the input force.

B Optimisation

B.1 Transcription

In single shooting, the equation of motion can be integrated (with Euler, or Runge-Kutta) over the whole trajectory. Events are detected and processed along the way. Due to the integration from start to end (single shoot), mapping between control, dynamics, costs and constraints can be highly non-linear, which degrades the convergence behaviour of the optimisation. This can be improved by dividing the integration into segments that are evaluated separately, multiple shooting. By re-starting the integration, the mapping is less non-linear, which improves the performance of the optimisation. Although the size of the optimisation is increased by additional constraints to ensure continuity between the segments [1].

If the lengths of the segments are equal to the step-size of the numerical integration, integration becomes unnecessary, and the constraint violations can be expressed analytically. With direct collocation this is done and intermediate states are defined by a polynomial of degree d, which ensures that the solution is smooth. At the bounds of segments, continuity is enforced. Increasing accuracy is achieved by either increasing the number of segments or the order of the polynomial [2]

B.2 Multiphase

Many trajectory optimization problems have a sequence of continuous-motion phases separated by discrete jumps. The gait of legged locomotion has a discontinuity at each foot strike on the ground. Solving a multiphase problem can be considered as solving multiple single-phase problems in parallel. The key difference is that the boundary constraints between any two phases can be connected, thus coupling the trajectory segments. In B.1 an overview is displayed with the stages and stage transitions.

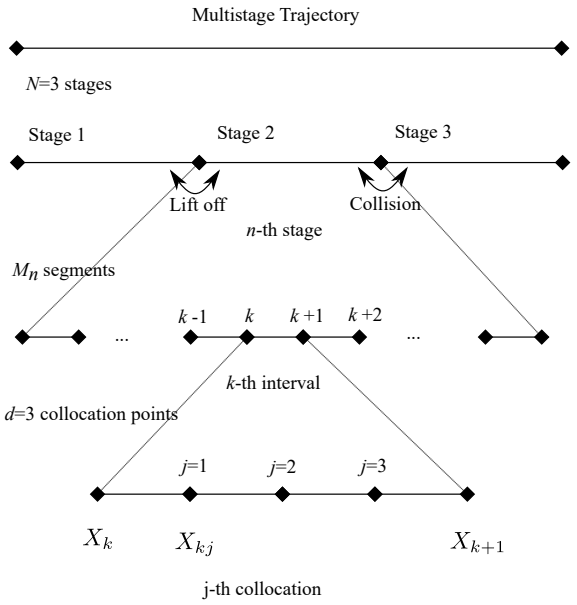

Figure B.1: Scheme showing multiphase optimization transcribtion

B.3 Collocation

In direct collocation, intermediate states are defined at collocation points as variables. The collocation points ¿ are a fraction of step size h_k. The time points are

$$t_{k,j} = t_{k,1} + h_k \tau_j \quad \text{for} \quad k = 0,\ldots,n_k - 1 \quad \text{and} \quad j = 0,\ldots,d \tag{B.1}$$

where ¿ is given at d collocation points. The amount of points is equal to degree of the polynomials. We choose the time points for Legendre collocation points (example for $d = 3$)

$$\tau = \begin{bmatrix} 0.0 & 0.1127 & 0.500 & 0.8872 \end{bmatrix} \tag{B.2}$$

For each control interval we define Lagrange polynomial basis.

$$L_j(\tau) = \prod_{r=0, r\neq j} \frac{(\tau - \tau_r)}{(\tau_j - \tau_r)} \tag{B.3}$$

We use Legendre polynomial coefficients because they have same variable bounds as the profiles themselves.

The Lagrangian basis satisfies

$$L_j(\tau_r) = \begin{cases} 1, & \text{if } j = r \\ 0, & \text{otherwise} \end{cases} \tag{B.4}$$

The estimate of the state as a linear combination of basis functions can be described by

$$\tilde{x}_k(t) = \sum_{r=0} L_r\left(\frac{t - t_k}{h_k}\right) x_{k,r} \tag{B.5}$$

We can write the state estimations the time derivative at each collocation point

$$\begin{aligned} \dot{\tilde{x}}_k(t_{k,j}) &= \frac{1}{h_k} \sum_{r=0} \dot{L}_r(\tau_j)\, x_{k,r} \\ &\stackrel{\text{def}}{=} \frac{1}{h_k} \sum_{r=0} C_{r,j}\, x_{k,r} \end{aligned} \tag{B.6}$$

The state at end of the control interval is

$$\begin{aligned} \tilde{x}_{k+1,0} &= \sum_{r=0} L_r(1) x_{k,r} \\ &\stackrel{\text{def}}{=} \sum_{r=0} D_r x_{k,r} \end{aligned} \tag{B.7}$$

The collocation equations need to be satisfied for every state at every collocation point

$$h_k f(t_{k,j}, x_{k,j}, u_k) - \sum_{r=0} C_{r,j} x_{k,r} = 0, \quad k = 0,\ldots,n_k - 1, \quad j = 1,\ldots,d \tag{B.8}$$

The continuity equation has to be satisfied on every control interval

$$x_{k+1,0} - \sum_{r=0} D_r x_{k,r} = 0, \quad k = 0,\ldots,n_k - 1 \tag{B.9}$$

B.4 Pseudocode

The transcription of 1 phase is described in pseudocode in 1. It describes the implementation of the collocation scheme used. Where X_k are the states at control interval, U_k is control over the control interval, S_k are the slack variables, X_{kj} are the states at the collocation points.

Algorithm 1 Collocation transcription of non-linear constrained optimisation

X_k ▷ Initial state variable
for $k \text{Æ} 0 : N \text{ i } 1$ **do** ▷
  U_k ▷ New control variable
  for $j \text{Æ} 1 : d$ **do** ▷ Create collocation points
    X_{kj} ▷ New state variable at collocation points
    S_{kj} ▷ New slack variable
  end for
  $X_{k,end} \text{Æ} D(1) X_k$ ▷ Loop over collocation points
  for $j \text{Æ} 1 : d$ **do**
    $x_p \tilde{A} C(1, j \text{Å} 1) X_k$ ▷ State derivative at collocation point
    for $r \text{Æ} 1 : d$ **do**
      $x_p \tilde{A} x_p \text{Å} C_{r \text{Å} 1, j \text{Å} 1} X_{kj}(r)$
    end for
    $f \tilde{A} f(X_{kj}, U_k)$ ▷ Append collocation equation state
    $q_j \tilde{A} f(X_{kj}, U_k)$ ▷ Append collocation equation quadrature
    $h f \text{ i } x_p \text{Æ} 0$ ▷ equality constrain
    $X_{k,end} \tilde{A} X_{k,end} \text{Å} D_{j \text{Å} 1} X_{kj}$ ▷ Add contribution to end state
    $J \tilde{A} J \text{Å} B_{j \text{Å} 1} q_j h$ ▷ Add contribution to quadrature function
  end for
  X_k ▷ New state variable at end of interval
  $X_{k,end} \text{ i } X_k \text{Æ} 0$ ▷ equality constrain
end for

Bibliography

[1] M. Kelly, "An introduction to trajectory optimization: How to do your own direct collocation," *SIAM Review*, vol. 59, no. 4, pp. 849–904, 2017.

[2] J. T. Betts, *Practical methods for optimal control and estimation using nonlinear programming*. SIAM, 2010.